Among the recombinant TSPOs, the BcTSPO

Leeyah Issop, Luminita Duma, Stephanie Finet, Olivier Lequin, Jean-Jacques Lacapère

Among the recombinant TSPOs, the *Bc*TSPO

Leeyah Issop[1], Luminita Duma[2], Stephanie Finet[3], Olivier Lequin[4] and Jean-Jacques Lacapère[4]

1 Inserm U955-IMRB, UPEC, Ecole Nationale Vétérinaire d'Alfort, F-94010 Créteil, France.
2 University of Reims Champagne-Ardenne, CNRS, ICMR UMR 7312, 51687 Reims, France
3 IMPMC, UMR 7590 CNRS, Sorbonne Université, MNHN, IRD, 75005 Paris, France
4 Sorbonne Université, Ecole normale supérieure, PSL University, CNRS, Laboratoire des Biomolécules, LBM, 75005 Paris, France

Abbreviations:

ALA δ-aminolevulinic acid
BcTSPO Bacillus cereus TSPO
CAT Chloramphenicol Acetyl Transferase
DDM Dodecyl-β-D-maltoside
DPC Dodecylphosphocholine
EC50 Efficient concentration
HPLC High Pressure Liquid Chromatography
IB inclusion bodies
IMAC Immobilized Metal Affinity Chromatography
MB membrane
NiNTA Nickel nitrilotriacetic acid
NMR Nuclear Magnetic Resonance
PPIX Protoporphyrin IX
ROS Reactive Oxygen Species
RsTSPO Rhodobacter sphaeroides TSPO
SDS Sodium Dodecyl Sulfate
SDS-PAGE SDS polyacrylamide gel electrophoresis
TSPO Translocator protein
WB Western Blot

Highlights

- Hemin is bound to *Bc*TSPO overexpressed in *E. coli*
- SDS-purified *Bc*TSPO is structured and binds ligands
- Purified *Bc*TSPO is functional and degrades PPIX upon UV light irradiation
- Oxygen-dependent PPIX degradation generates non-fluorescent products
- Products generated by ROS are hydroxyaldehydes

Graphical abstract

Summary

Overexpression of recombinant *Bacillus cereus* TSPO (*Bc*TSPO) in *E. coli* bacteria leads to its recovery with a bound hemin both in bacterial membrane (MB) and inclusion bodies (IB). Unlike mouse TSPO, *Bc*TSPO purified in SDS detergent from IB is well structured and can bind various ligands such as high-affinity PK 11195, protoporphyrin IX (PPIX) and δ-aminolevulinic acid (ALA). For each of the three ligands, ^{1}H-^{15}N HSQC titration NMR experiments suggest that different amino acids of *Bc*TSPO binding cavity are

involved in the interaction. PPIX, an intermediate of heme biosynthesis, binds to the cavity of *Bc*TSPO and its fluorescence can be significantly reduced in the presence of light and oxygen. The light irradiation leads to two products that have been isolated and characterized as photoporphyrins. They result from the addition of singlet oxygen to the two vinyl groups hence leading to the formation of hydroxyaldehydes. The involvement of water molecules, recently observed along with the binding heme in *Rhodobacter sphaeroides* (*Rs*TSPO) is highly probable. Altogether, these results raise the question of the role of TSPO in heme biosynthesis regulation as a possible scavenger of reactive intermediates.

Keywords:
Membrane protein
Functional Recombinant TSPO
Hemin
Porphyrin
Aminolevulinic acid

1. Introduction

TSPO is a highly conserved transmembrane protein found in most species from bacteria to human [1]. TSPO is encoded by non-essential genes that are upregulated in cells [2]. Its implication has been described in many diseases but precise functions in several organisms and cells remain elusive. TSPO expressed in native *Rhodobacter sphaeroides* and *Bacillus cereus* bacteria have been described to regulate tetrapyrrole metabolism [3,4]. It has been highlighted that purified recombinant bacterial TSPO could have enzymatic properties of protoporphyrin (PPIX) degradation upon light activation [5–7] but the mechanism underlying such a degradation process remains unknown and raises a couple of other questions: How do the reactive oxygen species (ROS) generated by light activate the PPIX cleavage? Does this mechanism lead to a dead-end complex [7]? How does the PPIX binds to TSPO? Various studies show the implication of transmembrane helices (TM1 and TM2) as well as cytosolic loops in the ligand binding [7–11]. More generally, does TSPO have several different conformations with and without ligand? NMR data of mouse TSPO (mTSPO) in dodecylphosphocholine (DPC) detergent suggest that the high-affinity drug ligand, PK 11195, stabilizes one "close" conformation [12] whereas several conformations are observed without ligand in DPC [13] as well as reconstituted in lipid membranes [14]. Surprisingly, X-ray data of bacterial TSPOs in lipid cubic phase do not show large structure conformational differences between the atomic structures with and without PK 11195 [6], porphyrin [15] or heme [7]. One potential hypothesis to these structural data might be the presence of different native conformational flexibility between the mammalian and bacterial TSPOs [13]. A second hypothesis claims that the occurring folding upon detergent treatment is different compared to the one in lipid environment [16,17]. It has also been suggested that protein motions differ substantially between detergent and lipid environment [18]. Solid-state NMR studies on mTSPO in a lipid environment revealed that the protein adopts different conformations depending on the presence or absence of PK 11195 [14,19,20] or the presence of cholesterol [21]. Thus, to gain a better understanding of the

native TSPO folding between different organisms, structural studies of bacterial TSPO in detergent would be beneficial.
Overexpression of *Bacillus cereus* (*Bc*TSPO) in *E. coli* bacteria generates proteins located in the membrane that have been purified with dodecylmaltoside (DDM) and used to get three-dimensional crystals in lipid cubic phases [6]. Spin-label double electron-electron resonance experiments indicate that *Bc*TSPO with or without PPIX, adopts different conformations in membrane scaffold protein (MSP)-based lipid nanodiscs from the crystal structures [11]. In the present study, we show that overexpression of *Bc*TSPO in *E. coli* bacteria leads to two pools of proteins: one in the cytosolic membranes and the other one , in a larger amount in the inclusion bodies . Both purifications, in DDM (for the protein in the cytosolic membranes) and SDS (for the protein in inclusion bodies), revealed the presence of a hemin associated with the *Bc*TSPO and therefore raises questions about its role or function. We further show that the SDS-purified *Bc*TSPO is structured and functional since it binds and degrades PPIX upon light irradiation, suggesting a potential regulation function.

2. Material and methods

Expression and purification of BcSPO: From an initial glycerol stock of BL21 (DE3) pLysS cells containing *Bc*TSPO cDNA cloned into a pETM-11/LIC vector (*generous gift of H. Nury & F. Dupeux, IBS Grenoble*), *Bc*TSPO expressing bacteria were grown in 3 L of Lysogeny Broth (LB) or minimal (M9) medium supplemented with 50 µg/mL of kanamycin and 25 µg/mL of chloramphenicol at 37 °C. After an overnight preculture, IPTG at 1 mM final concentration, was added and incubated for 18 hours at 20 °C. Cells were harvested by centrifugation (6.700×g, 20 min) at 4 °C and resuspended in a buffer containing 50 mM Hepes NaOH, 300 mM NaCl, pH 7.8 and lyzed by sonication.
Inclusion bodies and membrane fragments were separated by centrifugation at 15000×g for 30 minutes at 20 °C. The pellet containing *Bc*TSPO in inclusion bodies was solubilized with 1% of SDS. Insoluble material was removed by centrifugation at 50,000×g for 1h. The supernatant containing *Bc*TSPO in membranes was centrifuged at 100,000×g at 4°C, by adding DDM at 0.8% final concentration. Benzonase was added to each supernatant prior to the purification using a NiNTA column preequilibrated with buffer supplemented with the specific detergent. Protein fractions were eluted in the same buffer complemented with 200 mM of imidazole and each fraction was analysed by UV spectrometry.

Dialysis: 20 mM sodium phosphate buffer at pH 6.5 supplemented with 0.2% SDS or 0.05% DDM was used to dialyse the purified samples of *Bc*TSPO through Spectra/Por dialysis membranes (MWCO 6-8,000 Da cutoff).

UV-VIS Spectrophotometry: UV spectra were recorded on a UV-Visible (UNICAM UV300 spectrophotometer). Protein amounts were quantified by measuring absorbance at 280 nm using the epsilon 2.64 mL $mg^{-1}cm^{-1}$ or 56,380 $M^{-1}cm^{-1}$ calculated from the sequence of the recombinant protein. Presence of tetrapyrroles was analyzed by recording the UV-visible spectrum up to 500 nm that led to the observation of an absorbance peak at 408 nm.

Analysis by SEC and FPLC: Gel filtration of SDS-extracted and dialyzed *Bc*TSPO was performed on Superdex 200^{TM} 10-300 GL column using AKTA-FPLC system (GE Healthcare) at a flow rate of 0.3 mL/min.

NaPPIX solution preparation: A stock solution of protoporphyrin sodium salt, NaPPIX (Sigma Aldrich 258385), was freshly made at a concentration of 1-3 mM by dissolving weighting powder in a 0.1 mM NaOH solution. Higher concentrations (as high as 30 mM in the same medium) have been carefully prepared taken since NaPPIX molecules tend to stack at high concentration leading to slow kinetics of dissociation. This can be reduced by adding detergent in the stock solution at a concentration used for biochemical and/or biophysical studies. NaPPIX stock solution concentration was determined in acidic medium (HCl 1 M) using an extinction coefficient of 262,000 $M^{-1}cm^{-1}$ at 408 nm [22] that corresponds to the Soret band. Figure S1 shows that absorbance of NaPPIX is highly dependent on the pH of the medium (HCl, H_2O, NaOH) as well as its hydrophobicity (DMSO versus phosphate buffer) and is only weakly affected by the presence of detergent. It also shows that PPIX fluorescence intensity changes with the medium.

Fluorescence measurements: Intrinsic fluorescence of *Bc*TSPO was measured with excitation wavelength set at 290 nm and emission spectra recorded with Biologic MOS 200 M equipment (Bio-Logic Science Instruments, France). DPC titration was performed by adding increasing amounts of a 20% stock solution and recording spectra. Titration curve was fitted using the following equation $\Delta F=\Delta F_{max}*[DPC]/(EC_{50}+[DPC])$. NaPPIX fluorescence emission spectra were recorded between 580 and 720 nm with excitation set at 405 nm. Kinetics used for titration were recorded with excitation and emission wavelengths set at 405 and 630 nm, respectively. The K_{app} was determined by curve fitting using the following equation $\Delta F=\Delta F_{max}*[PPIX]/(K_{app}+[PPIX])$. A 1 cm square quartz cuvette (Hellma) equipped with a stirrer was used to maintain solution homogeneous. 2 mL sodium phosphate 10 mM buffered at pH 6.5 was used as a blank.

Circular Dichroism analysis: Circular dichroism spectra were recorded on a Jobin-Yvon CD6 spectropolarimeter. Measurements were performed at room temperature using 1 mm path length quartz cuvettes (Hellman) for 2.5-5 µM *Bc*TSPO solubilized in 10 mM sodium phosphate buffer solution and 0.2% SDS or 0.2% DPC. CD spectra were recorded from 185 to 270 nm wavelength with 0.2 nm step resolution, 1 s signal averaging and 1 nm bandwidth. Spectra were averaged over five scans, corrected for baseline and smoothened over 25 points. Spectral deconvolution was performed with CDPRO software [23].

UV irradiation: Time dependent UV irradiation was performed with a Spectrolinker (TM) XL-1000 that contains 3 tubes of 8 watts giving 254, 312 and 365 nm, respectively. Full power was 1.5 mW/cm^2.

Analysis by HPLC: Solutions of irradiated and non-irradiated PPIX were analyzed on a C18 column (4.6×100 mm, 300 Å, 3 µm proto 200 Higgins Analytic) and eluted at 1 mL/min with acetonitrile gradient in the presence of 0.1% TFA on a Dionex Ultimate 3000. The compounds fraction 1 (F1) and fraction 2 (F2) from irradiated PPIX were separated on preparative C18 column (10×250 mm, 300 Å, 5 µm); solvent was eliminated

with a rotary evaporator, fractions were lyophilized and resuspended in 600 µL of deuterated DMSO for NMR and mass spectrometry characterizations.

Mass spectrometry: ESI-QTOF-MS (Agilent, France) was performed on the Mass spectrometry platform of the Enzyme and Cell Engineering UMR 7025 CNRS laboratory, University of Technology of Compiègne, France. Ion mobility mass spectrometry permits to assign ion *m/z* 594.248 to a compound $C_{34}H_{34}N_4O_6$ and its $(M+H)^+$ at *m/z* 595.2559 to $C_{34}H_{35}N_4O_6$ for F1 major peak whereas the ion *m/z* 594.2449 was assigned to a compound $C_{34}H_{34}N_4O_6$ and its $(M+H)^+$ at *m/z* 595.2559 to a compound $C_{34}H_{35}N_4O_6$ for F2.

NMR spectroscopy: All NMR spectra were recorded on a Bruker NMR spectrometer equipped with a 5 mm TCI cryoprobe operating at 500 MHz ^1H Larmor frequency. Temperature has been regulated at 40°C using a Bruker variable temperature (BVT) unit. 2D ^1H-^{15}N HSQC spectra were recorded on 0.1 mM *Bc*TSPO samples in 10 mM sodium phosphate buffer pH 6.5, 90:10 H_2O:D_2O solutions containing 0.2% SDS and medium was complemented with DPC up to 10% final concentration. For ligand titration, NaPPIX was added from 3 mM stock solution, PK 11195 was added from dry films, and ALA from 20 mM stock solution. 1D ^1H, 2D ^1H - ^1H TOCSY and 2D ^1H - ^{13}C HSQC spectra of NaPPIX and irradiated NaPPIX were recorded in DMSO-d_6.

3. Results and discussion

3.1. Expression and purification of *Bc*TSPO

Previous overexpression of *Bc*TSPO in bacteria was performed in Terrific Broth (TB) medium at 20 °C with overnight induction [6]. This generates large amounts of bacteria (typically with OD_{600} culture above 8) but culture can also be performed successfully at higher temperature or in other media such as Lysogeny Broth (LB) or minimal medium (M9), the latter being needed for isotope ^{15}N, ^{13}C labeling in NMR studies.

Bacterial fractionation revealed that *Bc*TSPO is encountered both in membranes fraction (MB) and in inclusion bodies (IB) and can be purified using either DDM or SDS for MB or IB, respectively. Figure 1 shows absorption spectra of elution fractions from IMAC purification of MB (Figure 1A) and IB (Figure 1B). Both spectra bring to light the presence of a peak around 408 nm characteristic of tetrapyrrole. We recorded fluorescence spectra of the samples and the absence of fluorescence around 600 nm suggesting that the bound compound is not Uroporphyrin, Coproporphyrin or PPIX since all these compounds exhibit specific fluorescence when excited at 400-408 nm [24]. The bathochromic shift in UV/Vis absorption spectra [25,26] after the sodium dithionite treatment, which reduces ferric iron (Fe^{3+}) in hemin into ferrous iron (Fe^{2+}) in heme, provides evidence of a hemin bound to *Bc*TSPO prior to dithionite treatment (Figure 1C). The absorbance ratio 280/410 is close to 4 and 3 for MB and IB, respectively. This rough estimation suggests that *Bc*TSPO purified from MB with DDM seems to contain more tetrapyrroles than *Bc*TSPO purified from IB with SDS. Thus, protein found in the IB seems to originate from protein metabolic degradation rather than misfolded addressing. However, this different ratio of hemin over protein is not clear and may originate from: (i) the bacterial metabolism, the MB bound *Bc*TSPO may lose hemin when addressed to IB, (ii) the purification, hemin may

dissociate differentially from MB and IB fractions along with dilution steps, due to detergent specificities (DDM is known to be a milder detergent than SDS) (iii) the contribution of contaminant proteins containing hemin in the MB fractions that exhibit a reduced purity compared with IB fractions, cannot be excluded (Figure 1D).

Interestingly, dialysis of *Bc*TSPO purified from the IB fraction didn't lead to hemin removal as confirmed by the conservation of the absorbance peak at 408 nm after dialysis. Instead, overnight incubation of MB fraction before DDM extraction leads to the loss of bound hemin. This observation suggests that the SDS solubilized *Bc*TSPO from IB exhibits a binding of hemin which is tighter than the one when *Bc*TSPO is extracted with DDM from MB.

The amount of total protein recovered from IB is almost ten times higher and also more pure than the one recovered from MB (Figure 1D). A previous study [6] showed that a second step of purification after concentration was needed to get enough protein suitable for crystallography from DDM membrane purified fraction. However, the concentration step seems to induce the formation of different oligomeric states capable to crystallize but none of them have a tetrapyrrole bound [6]. On one hand, this highlights that the oligomeric form is not essential for crystallization but also, on the second hand, that the tetrapyrrole is not tightly bound and probably lost during the various steps of purification and/or crystallization. This finding is consistent with the function, previously described for bacterial TSPO in enzymatic PPIX degradation [5], of tetrapyrrole binding and release after light irradiation. Since crystal formation is a slow process, it allows sufficient time to the tetrapyrrole to be released [6]. We observed that the tetrapyrrole bound to the DDM purified *Bc*TSPO can be lost over time during purification steps prior to IMAC purification. Moreover, extensive washing of tetrapyrrolebound *Bc*TSPO purified protein, before elution, also tends to remove bound porphyrin.

To further characterize the localization of *Bc*TSPO in the *E. coli* membrane, we separated inner and outer membrane (Figure S2A) on sucrose gradient [27] (Figure S2B). Purification of each collected fraction revealed the presence of *Bc*TSPO with a bound hemin (Figure S2C) and western blot (WB) further confirmed that the band corresponds to the protein *Bc*TSPO (Figure S2D). Overexpression of *Rs*TSPO in *E. coli* bacteria was predominantly observed in the inner membrane [28]. This might be due to the overexpression process, since a previous study on native *R. sphaeroides* bacteria has shown by WB that *Rs*TSPO is in the outer membrane of the Gram negative bacteria [29]. The orientation of the protein within the bacterial membrane is not fully described compared to mitochondria where the C-terminus was characterized to face the cytoplasm [30]. For bacteria, predicted topology based on hydropathy analysis and the "positive inside" rule suggested for *Rs*TSPO an orientation of the inserted protein with the C-terminus facing the cytoplasm [28]. Similar results were obtained for TSPO from other bacteria like *P. fluorescens* using the software PSORTb [31].

SDS-PAGE for *Bc*TSPO purified from IB shows an additional band (Figure 1D) that we attempted to identify. We hypothesize that the two bands could correspond to *Bc*TSPO with different bound porphyrin content and/or complex conformations. However, NaPPIX addition to purified *Bc*TSPO does not generate a specific band in SDS-PAGE or a change in the ratio between the two bands. We checked any possible contaminant protein. Indeed, the IMAC purification from a bacterial culture without IPTG induction allowed to purify a 25 kDa protein that could correspond to the *E. coli* bacterial protein CAT

(Chloramphenicol acetyltransferase) or YadF (carbonic anhydrase) previously described as commonly copurified on NiNTA column [32]. The former (CAT) catalyses the formation of chloramphenicol 3-acetate in line with the presence of chloramphenicol used for pLyS "resistance", the latter (YadF) has maximal expression in slow growing culture at high density conditions that we used. It must be noticed that this additional band is not always present in each preparation.

As previously described for overexpressed *Bc*TSPO in MB purifications [6], we observed, in the SDS-PAGE, higher molecular weight bands for some purifications of *Bc*TSPO from IB (Figure S3A). Their characterization by size exclusion chromatography (Figure S3B) reveals the presence of a main peak at ~11 mL (corresponding to the monomer), but also a smaller peak at ~10 mL that may be attributed to oligomers of several sizes as seen in the gels. It must be mentioned that the monomer/dimer ratio was not the same in all purifications which might be associated with unintended variations in the purification protocol.

In conclusion, when overexpressed in *E. coli* bacteria, *Bc*TSPO is found both in MB and IB, but purification of the latter leads in a single step to a more concentrated and mostly pure protein with a bound hemin.

3.2. Structural studies

TSPOs are tryptophan rich membrane proteins that permit fluorescence studies. Intrinsic fluorescence of *Bc*TSPO in SDS (Figure 2A) purified from IB suggests that the detergent surrounding the protein can be exchanged with DPC, hence leading to a large increase of the intrinsic fluorescence, as previously described for mTSPO [17,19]. This fluorescence increase is due to a change in the tryptophan environment, and for mTSPO, it has also been correlated with secondary structure changes [17,19]. Unlike previous mTSPO observations, CD of *Bc*TSPO (Figure 2B) reveals that the SDS exchange with DPC does not induce a significant change in CD signal, and therefore in the secondary structure. This result suggests that *Bc*TSPO folding is less affected by the detergent and probably that *Bc*TSPO does not exist as a large heterogeneous mix of conformations as suggested for free mTSPO protein [13,14]. Spectra deconvolution revealed that *Bc*TSPO is highly folded in alpha helices (Table 1).

NMR analysis of proteins requires stable isotope labelled samples. To produce them, prior its extraction from IB, *Bc*TSPO was expressed in a ^{15}N-enriched medium which further allowed the recording of a 2D ^{1}H - ^{15}N HSQC spectrum of *Bc*TSPO in SDS (Figure 3A). The distribution of the correlations in the spectrum suggests a better folding of *Bc*TSPO protein unlike apo mTSPO under the same purification conditions [19]. This improved folding might be correlated to the presence of the hemin ligand. The indole region displays several individual peaks, but more than the 7 expected given the number of tryptophans (W) present in the protein sequence. Similarly, the glycine (G) region contains more peaks than could be expected for 6 residues. Finally, the *Bc*TSPO has only one arginine (R), but several cross-peaks are observed for the NH^{ε} and NH^{η}. This can be due to the specific location of this residue in the loop linking TM1 and TM2, which may be affected by the existence of different conformations. This amino acid has been previously shown to be involved in the binding of PK 11195 to mTSPO [8]. Addition of DPC induces an important change in the ^{1}H - ^{15}N HSQC spectrum (Figure 3B) as previously described for mTSPO [13,19]. In addition, we observe a down field shift (i.e., high chemical shift) of

the indole peaks, fewer correlations in the "glycine" region and the disappearance of the correlations assigned to the $NH^{\varepsilon}/NH^{\eta}$ of R. These changes suggest that DPC addition affects the interconversion dynamics between the different protein conformations.

Titration of TSPO ligands (PK 11195, PPIX or ALA, delta aminolevulinic acid, known as heme precursor) into ^{15}N labeled *Bc*TSPO purified in SDS induces changes in the ^{1}H - ^{15}N HSQC spectrum (Figure 4). Excerpts from the indole region show that addition of PK 11195 has the highest effect when compared to other two ligands. The addition of PK 11195 affects differently the sidechains of the W residues when compared to that of PPIX (Figures 4A and 4B, respectively) whereas only few cross peaks are affected by presence of ALA (Figure 4C). As previously mentioned, *Bc*TSPO contains 7 W but more cross-peaks are observed in the indole region which supports the coexistence of several conformations. As in the case of PPIX titration into *Bc*TSPO, the presence of PK 11195 reduces the number of peaks suggesting less conformational heterogeneity. We also notice some peaks, like the one at 127 ppm, which undergo a change in their electronic environment (Figure 4A). It has been previously shown by X-ray crystallography [6] that PK 11195 binding in the *Bc*TSPO cavity notably involves hydrogen bonds with the indole of the 2 tryptophans (W51 and W138). The ligand is also in close proximity to the W31, which is part of the loop closing the cavity.

The PPIX-*Bc*TSPO complex structure has been previously generated by docking in the electrostatic potential surface of the binding cavity [6]. Ligand-protein contacts involve the tryptophans W51 and W138, and the docked structure of the complex shows that PPIX slightly protrudes out from the protein as observed for *Rs*TSPO (A139T)-PPIX complex [15]. This may indicate different interaction mechanisms between PK 11195 or PPIX with these W and the protein in general, since PPIX binds to mTSPO with lower affinity than PK 11195 does (K_i against PK 11195 ~0.5 µM) [33].

Previous observations that identified HsTSPO2 as an ALA transporter in cells [34] led us to probe the interaction between ALA and *Bc*TSPO (Figure 4C). In the indole region of ^{1}H - ^{15}N HSQC spectrum, only one peak is displaced suggesting a weak binding and a different interaction site or mechanism compared to PK 11195 and PPIX. The presence of ALA affects some other peaks (NH^{η}) corresponding to the single R (insert Figure 4C) and some glycines (not shown). It has to be noticed that the interaction of each ligand with *Bc*TSPO decreases the intensity of the NH^{η} R peak (inserts of Figure 4) suggesting the involvement of the loop linking TM1 and TM2 proposed to “close” the binding cavity [8].

Since the PPIX ligand is fluorescent, its binding to *Bc*TSPO has also been probed by monitoring the changes in its fluorescence (Figure 5A) in a titration experiment where the amount of PPIX increases. The observed variations in fluorescence intensity are attributed to an environment change of the PPIX which fluorescence increases in a hydrophobic environment such an organic solvent [35] linked to an increase of absorbance (Figure S1). Titration of this fluorescence increase, for free and *Bc*TSPO bound, permits to determine a stoichiometry of one mole of PPIX per *Bc*TSPO and apparent affinities in the micro molar range (Figure 5B), in agreement with inhibition studies against PK 11195 which lead to a K_i ~ 0.5 µM [33].

3.3. Functional studies

Previous studies have shown that different bacterial TSPOs can modify added PPIX upon light irradiation in the presence of dissolved oxygen and that the rate of PPIX

degradation depends on light intensity [5–7]. Indeed, Ginter and coworkers have shown that, upon increased light intensity, the reaction is faster and completely finished after 20 min [5]. *Bc*TSPO purified in SDS also cleaves PPIX as revealed by the decrease in PPIX fluorescence emission spectrum after increasing UV irradiation time (Figure 6A). Visible irradiation was ineffective to cleave PPIX alone (Figure 6B). The kinetics is faster in the presence of *Bc*TSPO with half time around 17 s (filled black circles in Figure 6C) than in its absence that occurs with a half time around 80 s (filled red squares). This enzymatic activity is similar when the protein is solubilized in SDS or in DPC (Figure 6D) but the kinetics have been slowed down (half time around 65 s) for a second addition of PPIX in the same cuvette (filled orange squares in Figure 6E). A third and fourth addition show, upon irradiation (filled grey triangles and yellow diamonds in Figure 6E), a fluorescence decrease with a kinetic behaviour similar to the one observed in the absence of *Bc*TSPO (Figure 6F). It has to be noticed that the rate of PPIX fluorescence decrease upon irradiation is constant in the absence of protein (Figure 6F) and not linearly dependent on the PPIX concentration. This means that the limiting step, in the presence of *Bc*TSPO, is the accumulation of PPIX product due to conversion of PPIX in its degradation product upon irradiation.

The product generated by irradiation of PPIX bound to *B*cTSPO has been previously called bilindigin because of its indigo color [6]. However, neither the corresponding mechanism nor the structure have been experimentally determined. The generation of bilindigin may be associated with an opening of the tetrapyrrole as it happens in living organisms by the formation of biliverdin that requires the heme oxygenase action, or by photooxidation as previously described for mesotetraarylporphyrin [36]. In order to identify and characterize the light-induced degradation, we collected the irradiated solution for chromatographic analysis and observed, as previously described [5], the appearance of two products more polar (Figure 7B) than PPIX (Figure 7A). The two purified compounds (Figure 7C) were analyzed by NMR. 2D ^{1}H – ^{1}H TOCSY (Figures 7D to G, Table 2) and ^{1}H – ^{13}C HSQC (not shown) spectra allowed to identify the two photoporphyrin compounds as two different hydroxyaldehydes generated by oxidation of one of the two vinyl groups [37]. The ^{1}H NMR signals of the four Meso hydrogens are well visible in the range 10 to 11 ppm and support no linearized degradation products. We can completely exclude the production of bilirubin, biliverdin or phycocyanobilin because the ^{1}H chemical shift of the Meso hydrogens in such linearized products appear between 3 and 8 ppm, depending of the compound (see Table 3). Oxidation reactions of one of the vinyl groups have been previously described under different media conditions as leading to at least five compounds whose proportions are controlled by the nature of the ROS, singlet oxygen and superoxide radical anion [38,39]. Among the five possible compounds, the major ones are generated via a singlet oxygen path [39]. The nature of photooxidation in biological systems is linked to oxygen diffusion and singlet oxygen lifetime [39]. These studies suggest that, if the porphyrin resides in a relatively hydrophobic site, the yield of the reaction of excited porphyrin with oxygen is governed by the residence time of the singlet oxygen in the site. Our data are in agreement with such a mechanism: on one hand, several atomic bacterial TSPO structures have revealed the presence of water molecules close or linked to porphyrin or heme in the binding cavity [6,7,15], that could generate ROS upon light irradiation; on the other hand, oxygen diffusion is slowed down in hydrophobic media compared to water [39]. In summary, we propose that PPIX bound in *Bc*TSPO cavity

tightly interacts with water molecules. UV irradiation generates excited porphyrin and ROS (Figure 8A), such as singlet oxygen that reacts with vinyl groups, leading to the formation of two different hydroxyaldehydes that do not fluoresce (Figure 8B). The absence of these vinyl groups in Uroporphyrin and Coproporphyrin explains why they are not "substrates" of *Ct*TSPO, as previously described [5]. The reaction of PPIX with oxygen upon UV irradiation modifies the pyrrole group that becomes pyrrolidine and probably induces a "kink" in the tetrapyrrole ring. Without irradiation, the latter is almost flat as observed, for example, in the porphyrin bound to cytoperoxydase (Figure 8C). The loss of fluorescence of the compounds produced by UV irradiation is probably due to the loss of the π-electron delocalization over the conjugated double-bond system that is disrupted by the modification of one of the pyrroles moieties. The degraded porphyrin characterized in the crystal structure of *Rs*TSPO reveals a highly distorted structure in agreement with our observations (Figure 8D).

At the molecular level, previous structural studies have shown that several amino acids of the TSPO are in interaction with PPIX or heme [6,7,11,15]. Some π-π interactions between heme and aromatic residues, and hydrogen bonds involving water molecules have also been described recently [7]. PPIX docking in the *Bc*TSPO showed W31, W40, W51 and W138 as candidates to interact with vinyl groups [6]. W51 and W138 located in transmembrane domains are closer to one vinyl whereas W31 and W40 located in the first loop are closer to the other vinyl (Figure 9A). The involvement of this loop in the stabilization of PPIX-*Bc*TSPO complex has been recently described by electron spin resonance and mutagenesis studies [11]. These environment differences could explain the different ratio of the two hydroxyaldehydes obtained. The amino acid sequence comparison between species (Figure 9B) shows that W40 and W138 are conserved in bacterial and human TSPO (*Bc*TSPO, *Rs*TSPO, *Ct*TSPO, HsTSPO1 and HsTSPO2). W31 is almost conserved since it is replaced by a Y but preceded by a W in the sequence of *Ct*TSPO. W51 is less conserved since it is replaced by Q in HsTSPO2. Recent atomic structure of *Rs*TSPO with a bound heme [7] shows (Figure 9A right) that the two vinyl groups interact with a water molecule that makes a bond with W50 and W135 of *Rs*TSPO.

Mutation of W51F in *Bc*TSPO has been described to lead to a different PPIX light irradiation product with fluorescence spectra having a 673 nm fluorescence band [6,11], which raises the question of a potentially different activity between WT and mutated *Bc*TSPO. Nε of W51 in the WT interacts with vinyl of PPIX and probably stabilize it within the cavity. The W51F mutant, which does not have the nitrogen, has a different binding cavity that probably changes the interaction between PPIX and *Bc*TSPO [11]. Therefore, the irradiation may lead to different compound(s) compared to those characterized herein. The origin of this fluorescence remains unexplained and needs further studies.

Two mutants of *Ct*TSPO (W142F and A147T, sequence of 159 amino acids) were described to lose the capacity to modify PPIX upon light irradiation in the presence of dissolved oxygen [5]. The first one (W143 in Figure 9B) is a conserved W that may interact with the =CH Meso of porphyrin as characterized in *Rs*TSPO atomic structures (PDB code 8E7W or 8E7X) by distances of 5.8 Å or 6.0 Å and having a water molecule in between. The second one (A147 in Figure 9B) is a conserved amino acid involved in the natural polymorphism of mammalian TSPO that leads to differential binding of PET radioligands [40]. PPIX was not degraded upon light irradiation neither in the presence of HsTSPO1

mutant (A147T) nor of HsTSPO2 that contains this "native A/T mutation" [6]. When replaced by T in *Rs*TSPO (A139T), this latter mutant has been recently shown to bind only one PPIX per dimer and to retain degraded PPIX in the cavity [7] suggesting the involvement of this conserved Ala in the potential modification of PPIX. The difference between species might be due to a variation in the local amino acids positions.

4. Conclusion

Recombinant *Bc*TSPO has been successfully overexpressed in *E. coli* bacteria and purified in detergent from both membrane and inclusion bodies. Previous results in the literature revealed that the ligand was lost during purification or crystallization (that may take several days), explaining therefore why the ligand is not observed in the *Bc*TSPO X-ray structure [6]. We suspect that this may also happen for *Rs*TSPO demonstrating why only one PPIX is observed per dimer [15]. We show that *Bc*TSPO purified from IB or MB is able to degrade PPIX in a light- and oxygen-dependent manner as previously described for other bacterial TSPOs [5-7]. This might explain why a "distorted" PPIX has been characterized in *Rs*TSPO crystals [15]. The NMR derived structure of the UV-oxygen degraded compounds shows that the two vinyl groups, are: i) deeply buried into the protein cavity, as previously observed for bound heme in *Rs*TSPO and PPIX docked in *Bc*TSPO, and ii) transformed in aldehydes, hence explaining the loss of PPIX fluorescence properties upon UV irradiation. Such process probably involves water molecules as previously observed by crystallography in the ligand binding cavity. All these data raise the question of the potential role of TSPO in the metabolism of heme (Figure 10). Is TSPO a cytosolic heme scavenger as previously described in plants [2]? For the moment the question remains open and further work is needed to answer it.

Acknowledgments

We thank Hugues Nury and Florine Dupeux (IBS Grenoble) for the generous gift of BL21 pLysS cells containing *Bc*TSPO cDNA cloned into a pETM-11/LIC vector. We acknowledge Bruna Seferian, Agathe Berniguet, Quentin Palanque, Daniela Rodriguez-Braz, Farah Oueslati, Mohyeddine Taleb and Charline Henriot for technical help in the expression and the purification of *Bc*TSPO. We also acknowledge Rodrigue Marquant for HPLC experiments and Franck Merlier (UTC) for help with mass-spectrometry data recording.

References

[1] J. Fan, P. Lindemann, V. Papadopoulos, Structural and functional evolution of the translocator protein (18 kDa), Curr. Mol. Med. 12 (2012) 369–386.

[2] H. Batoko, V. Veljanovski, P. Jurkiewicz, Enigmatic translocator protein (TSPO) and cellular stress regulation, Trends Biochem. Sci. 40 (2015) 497–503. https://doi.org/10.1016/j.tibs.2015.07.001.

[3] A.A. Yeliseev, S. Kaplan, A novel mechanism for the regulation of photosynthesis

gene expression by the TspO outer membrane protein of Rhodobacter sphaeroides 2.4.1, J. Biol. Chem. 274 (1999) 21234–21243. https://doi.org/10.1074/jbc.274.30.21234.
[4] Y. Nitzan, M. Salmon-Divon, E. Shporen, Z. Malik, ALA induced photodynamic effects on Gram positive and negative bacteria, Photochem. Photobiol. Sci. 3 (2004) 430–435. https://doi.org/10.1039/b315633h.
[5] C. Ginter, I. Kiburu, O. Boudker, Chemical catalysis by the translocator protein (18 kDa), Biochemistry. 52 (2013) 3609–3611. https://doi.org/10.1021/bi400364z.
[6] Y. Guo, R.C. Kalathur, Q. Liu, B. Kloss, R. Bruni, C. Ginter, E. Kloppmann, B. Rost, W.A. Hendrickson, Structure and activity of tryptophan-rich TSPO proteins, Science. 347 (2015) 551–5. https://doi.org/10.1126/science.aaa1534.
[7] J. Liu, C. Hiser, F. Li, R. Hall, R.M. Garavito, S. Ferguson-miller, New TSPO crystal structures of mutant and heme-bound forms with altered flexibility, ligand binding, and porphyrin degradation activity, Biochemistry. 62 (2023) 1262–1273. https://doi.org/10.1021/acs.biochem.2c00612.
[8] S. Iatmanen-Harbi, L. Senicourt, V. Papadopoulos, O. Lequin, J.J. Lacapere, Characterization of the high-affinity drug ligand binding site of mouse recombinant TSPO, Int. J. Mol. Sci. 20 (2019). https://doi.org/10.3390/ijms20061444.
[9] A. Bruno, E. Barresi, N. Simola, E. Da Pozzo, B. Costa, E. Novellino, F. Da Settimo, C. Martini, S. Taliani, S. Cosconati, Unbinding of translocator protein 18 kDa (TSPO) ligands: From in vtro residence time to in vivo efficacy via in silico simulations, ACS Chem. Neurosci. 10 (2019) 3805–3814. https://doi.org/10.1021/acschemneuro.9b00300.
[10] T. Dixon, A. Uyar, S. Ferguson-Miller, A. Dickson, Membrane-mediated ligand unbinding of the PK-11195 ligand from TSPO, Biophys. J. 120 (2021) 158–167. https://doi.org/10.1016/j.bpj.2020.11.015.
[11] P. Yeh, C. Li, Y. Lu, Y. Chiang, Structural insights into the binding and degradation mechanisms of protoporphyrin IX by the translocator protein TSPO, J. Am. Chem. Soc. (2023). https://doi.org/10.1021/jacsau.3c00514.
[12] L. Jaremko, M. Jaremko, K. Giller, S. Becker, M. Zweckstetter, Structure of the mitochondrial translocator protein in complex with a diagnostic ligand, Science. 343 (2014) 1363–1367. https://doi.org/10.1126/science.1248725.
[13] Ł. Jaremko, M. Jaremko, K. Giller, S. Becker, M. Zweckstetter, Conformational flexibility in the transmembrane protein TSPO, Chem. - A Eur. J. 21 (2015) 16555–16563. https://doi.org/10.1002/chem.201502314.
[14] L. Duma, L. Senicourt, B. Rigaud, V. Papadopoulos, J.-J. Lacapère, Solid-state NMR study of structural heterogeneity of the apo WT mouse TSPO reconstituted in liposomes, Biochimie. (2022). https://doi.org/10.1016/j.biochi.2022.08.013.
[15] F. Li, J. Liu, Y. Zheng, R.M. Garavito, S. Ferguson-Miller, Crystal structures of translocator protein (TSPO) and mutant mimic of a human polymorphism, Science. 347 (2015) 555–558. https://doi.org/10.1126/science.1260590.
[16] F. Li, J. Liu, N. Liu, L.A. Kuhn, R.M. Garavito, S. Ferguson-Miller, Translocator protein 18 kDa (TSPO): An old protein with new functions?, Biochemistry. 55 (2016) 2821–2831. https://doi.org/10.1021/acs.biochem.6b00142.
[17] S. Combet, F. Bonneté, S. Finet, A. Pozza, C. Saade, A. Martel, A. Koutsioubas, J.J. Lacapère, Effect of amphiphilic environment on the solution structure of mouse

TSPO translocator protein, Biochimie. (2022). https://doi.org/10.1016/j.biochi.2022.11.014.
[18] L. Frey, N.A. Lakomek, R. Riek, S. Bibow, Micelles, bicelles, and nanodiscs: Comparing the impact of membrane mimetics on membrane protein backbone dynamics, Angew. Chem. Int. Ed. 56 (2017) 380–383. https://doi.org/10.1002/anie.201608246.
[19] J.J. Lacapere, S. Iatmanen-Harbi, L. Senicourt, O. Lequin, P. Tekely, R.N. Purusottam, P. Hellwig, S. Kriegel, S. Ravaud, C. Juillan-Binard, E.P. Peyroula, V. Papadopoulos, Structural studies of TSPO, a mitochondrial membrane protein, Membr. Proteins Prod. Struct. Anal. (2014) 393–421. https://doi.org/10.1007/978-1-4939-0662-8_14.
[20] L. Senicourt, L. Duma, V. Papadopoulos, J.J. Lacapere, Solid-state NMR of membrane protein reconstituted in proteoliposomes: the case of TSPO, in: J.J. Lacapère (Ed.), Membr. Protein Struct. Funct. Charact., Springer Protocols, Humana Press, 2017: pp. 329–344.
[21] G. Jaipuria, A. Leonov, K. Giller, S.K. Vasa, Á. Jaremko, M. Jaremko, R. Linser, S. Becker, M. Zweckstetter, Cholesterol-mediated allosteric regulation of the mitochondrial translocator protein structure, Nat. Commun. 8 (2017) 1–8. https://doi.org/10.1038/ncomms14893.
[22] C. Rimington, Spectral-absorption coefficients of some porphyrins in the Soret-band region, Biochem. J. 75 (1960) 620–623. https://doi.org/10.1042/bj0750620.
[23] N. Sreerama, R.W. Woody, Estimation of protein secondary structure from circular dichroism spectra: Comparison of CONTIN, SELCON, and CDSSTR methods with an expanded reference set, Anal. Biochem. 287 (2000) 252–260. https://doi.org/10.1006/abio.2000.4880.
[24] C.F. Polo, A.L. Frisardi, E.R. Resnik, A.E.M. Schous, A.M. del C. Battle, Factors influencing fluorescence spectra of free porphyrins, Clin. Chem. 34 (1988) 757–760.
[25] W. Liu, C.E. Rogge, B. Bambai, G. Palmer, A.L. Tsai, R.J. Kulmacz, Characterization of the heme environment in Arabidopsis thaliana fatty acid α-dioxygenase-1, J. Biol. Chem. 279 (2004) 29805–29815. https://doi.org/10.1074/jbc.M401779200.
[26] B.S. Francisco, E.C. Bretsnyder, R.G. Kranz, Human mitochondrial holocytochrome c synthase's heme binding, maturation determinants, and complex formation with cytochrome c, PNAS. 110 (2012) E788-797. https://doi.org/10.1073/pnas.1213897109.
[27] L.A. Baker, G.E. Folkers, T. Sinnige, K. Houben, M. Kaplan, E.A.W. Van Der Cruijsen, M. Baldus, Magic-angle-spinning solid-state NMR of membrane proteins, 1st ed., Elsevier Inc., 2015. https://doi.org/10.1016/bs.mie.2014.12.023.
[28] V.M. Korkhov, C. Sachse, J.M. Short, C.G. Tate, Three-dimensional structure of TspO by electron cryomicroscopy of helical crystals, Structure. 18 (2010) 677–687. https://doi.org/10.1016/j.str.2010.03.001.
[29] A.A. Yeliseev, S. Kaplan, A sensory transducer homologous to the mammalian peripheral-type benzodiazepine receptor regulates photosynthetic membrane complex formation in Rhodobacter sphaeroides 2.4.1, J. Biol. Chem. 270 (1995) 21167–21175. https://doi.org/10.1074/jbc.270.36.21167.
[30] E. Joseph-Liauzun, P. Delmas, D. Shire, P. Ferrara, Topological analysis of the

peripheral benzodiazepine receptor in yeast mitochondrial membranes supports a five-transmembrane structure, J. Biol. Chem. 273 (1998) 2146–2152. https://doi.org/10.1074/jbc.273.4.2146.
[31] A. Chapalain, S. Chevalier, N. Orange, L. Murillo, V. Papadopoulos, M.G.J. Feuilloley, Bacterial ortholog of mammalian translocator protein (TSPO) with virulence regulating activity, PLoS One. 4 (2009). https://doi.org/10.1371/journal.pone.0006096.
[32] V.M. Bolanos-Garcia, O.R. Davies, Structural analysis and classification of native proteins from E. coli commonly co-purified by immobilised metal affinity chromatography, Biochim. Biophys. Acta - Gen. Subj. 1760 (2006) 1304–1313. https://doi.org/10.1016/j.bbagen.2006.03.027.
[33] S. Taketani, H. Kohno, T. Furukawa, R. Tokunaga, Involvement of peripheral-type benzodiazepine receptors in the intracellular transport of heme and porphyrins, J. Biochem. 117 (1995) 875–880. https://doi.org/10.1093/oxfordjournals.jbchem.a124790.
[34] H. Manceau, S.D. Lefevre, A. Mirmiran, C. Hattab, H.R. Sugier, C. Schmitt, K. Peoc'h, H. Puy, M.A. Ostuni, L. Gouya, J.J. Lacapere, TSPO2 translocates 5-aminolevulinic acid into human erythroleukemia cells, Biol. Cell. (2020) 113–126. https://doi.org/10.1111/boc.201900098.
[35] B. Myrzakhmetov, P. Arnoux, S. Mordon, S. Acherar, I. Tsoy, C. Frochot, Photophysical properties of protoporphyrin IX, pyropheophorbide-a and photofrin® in different conditions, Pharmaceuticals. 14 (2021) 1–21. https://doi.org/10.3390/ph14020138.
[36] J. Wojaczyński, M. Popiel, L. Szterenberg, L. Latos-Grazyński, Common origin, common fate: Regular porphyrin and N-confused porphyrin yield an identical tetrapyrrolic degradation product, J. Org. Chem. 76 (2011) 9956–9961. https://doi.org/10.1021/jo201489z.
[37] R. Bonnett, G. Martinez, Photobleaching of sensitisers used in photodynamic therapy, Thetrahedron. 57 (2001) 9513–9547.
[38] G.S. Cox, D.G. Whitten, Mechanisms for the photooxidation of protoporphyrin IX in solution, J. Am. Chem. Soc. 104 (1982) 516–521. https://doi.org/10.1021/ja00366a023.
[39] G.S. Cox, M. Krieg, D.G. Whitten, Self-sensitized photooxidation of protoporphyrin IX derivatives in aqueous surfactant solutions: Product and mechanistic studies, J. Am. Chem. Soc. 104 (1982) 6930–6937. https://doi.org/10.1021/ja00389a008.
[40] D.R. Owen, A.J. Yeo, R.N. Gunn, K. Song, G. Wadsworth, A. Lewis, C. Rhodes, D.J. Pulford, I. Bennacef, C.A. Parker, P.L. Stjean, L.R. Cardon, V.E. Mooser, P.M. Matthews, E.A. Rabiner, J.P. Rubio, An 18-kDa Translocator Protein (TSPO) polymorphism explains differences in binding affinity of the PET radioligand PBR28, J. Cereb. Blood Flow Metab. 32 (2012) 1–5. https://doi.org/10.1038/jcbfm.2011.147.
[41] D. Chen, J.D. Brown, Y. Kawasaki, J. Bommer, J.Y. Takemoto, Scalable production of biliverdin IXα by Escherichia coli, BMC Biotechnol. 12 (2012). https://doi.org/10.1186/1472-6750-12-89.
[42] M. Suresh, S.K. Mishra, S. Mishra, A. Das, The detection of Hg2+ by cyanobacteria in aqueous media, Chem. Commun. (2009) 2496–2498.

https://doi.org/10.1039/b821687h.

Tables

Table 1: Secondary structure analysis of *Bc*TSPO CD spectra deconvoluted using CDPro software [23].

	Alpha	Beta	Turn	Random	Total
SDC	77.2	22.8	0	0	100
DPC	71.8	28.2	0	0	100

Table 2: ^{1}H, ^{13}C NMR chemical shifts of porphyrin compounds

	F2		F1		PPIX	
	^{1}H	^{13}C	^{1}H	^{13}C	^{1}H	^{13}C
CH=CHO	11.165 (1H, d, *J*=8.2)	n.d.	11.16 (1H, d, *J*=8.2)	n.d.	-	-
	8.01 (1H, d, *J*=8.2)	122.9	7.99 (1H, d, *J*=8.2)	122.9	-	-
=CH (Meso)	10.02 (1H, s)	100.0	10.01 (1H, s)	100.0	10.81 (1H, s)	98.7
	9.92 (2H, s)	98.5 93.7	9.97 (1H,s)	99.5	10.35 (1H, s)	97.7
	9.36 (1H, s)	91.3	9.86 (1H,s)	93.1	10.26 (2H, s)	97.3
	-	-	9.48 (1H,s)	91.3	-	
–CH=CH_2	8.44 (1H, dd, *J*=17.9, 11.7)	n.d.	8.32 (1H, dd, *J*=17.7, 11.6)	n.d.	8.53 (1H, dd, *J*=17.8, 11.0) 8.51 (1H, dd, *J*=17.8, 11.0)	130.3 130.3
	6.49 (1H, dd, *J*=17.8, 1.4)	n.d.	6.46 (1H, dd, *J*=17.7, 1.3)	n.d.	6.47 (1H, dd, *J*=17.8, 1.3)	121.4
	6.23 (1H, dd, *J*=11.6,1.4)	n.d.	6.24 (1H, dd, *J*=11.6, 1.1)	n.d.	6.46 (1H, dd, *J*=17.8, 1.3)	121.4
	-	-	-	-	6.23 (1H, dd, *J*= 11.5, 1.5)	121.4
	-	-	-	-	6.22 (1H, dd, *J*= 11.5, 1.5)	121.4
-CH_2-CH_2-	4.30 (2H)	21.3	n.d.	n.d.	4.32 (4H, t, J=7.3)	23.2
	3.15 (2H, t, *J*=7.5)	36.7	3.14 (2H, t)	n.d.	2.88 (4H, t, J=7.2)	40.6
	4.11 (2H)	21.3	n.d.	n.d.		
	3.08 (2H, t, *J*=7.5)	37.1	3.09 (2H, t)	n.d.		
CH_3	3.68 (3H, s)	n.d.	3.70 (3H, s)	n.d.	3.76 (3H, s)	12.7
	3.53 (3H, s)	n.d.	3.57 (3H,s)	n.d.	3.75 (3H, s)	12.7
	3.51 (3H, s)	n.d.	3.51 (3H, s)	n.d.	3.62 (3H, s)	11.2
	3.41 (3H, s)	n.d.	3.43 (3H,s)	n.d.	3.60 (3H, s)	11.2
NH	–2.55 (1H, s)	-	–2.67 (1H,s)	-	–3.83 (2H, s)	-
	–2.75 (1H, s)	-	–2.75 (1H,s)	-	-	-

Table 3: ^{1}H chemical shifts of the Meso hydrogens of PPIX, bilirubin, biliverdin and phycocyanobilin.

Compound	δ ^{1}H Meso (ppm)	Solvent	Reference
PPIX	10 – 11	DMSO-d_6	This work
Bilirubin	3.99	DMSO-d_6	10.13018/BMSE000627
Biliverdin	5.5, 6, 7.6	DMSO-d_6	[41]
Phycocyanobilin	3.35 – 3.65, 5 - 25	CDCl3	[42]

Figures

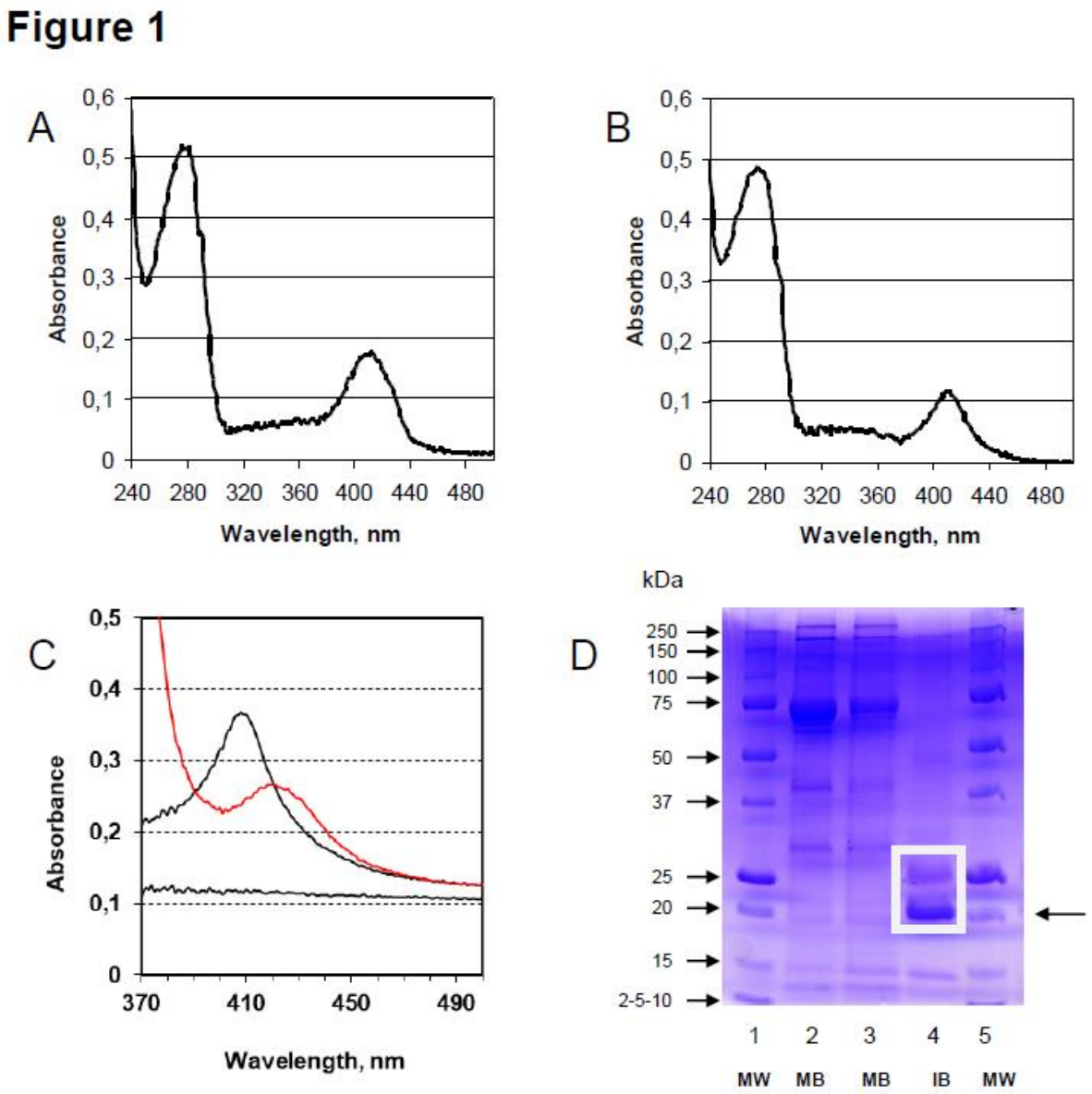

Figure 1: Purification of recombinant *Bc*TSPO. (**A and B**) Absorbance spectra of most concentrated elution fractions from IMAC purification of (**A**) MB in DDM detergent and (**B**) IB in SDS detergent. (**C**) Dithionite treatment of purified *Bc*TSPO shows a red shift of the absorption spectrum characteristic of the presence of a bound hemin. Black and red lines, before and after dithionite addition (few grains), respectively. (**D**) SDS-PAGE of purified fractions from MB and IB. Lanes 1 and 5, molecular weight standards, 2 and 3 MB fractions, 4 IB fraction. Arrow indicates *Bc*TSPO monomer. White box highlights the two major bands observed in IB samples.

Figure 2

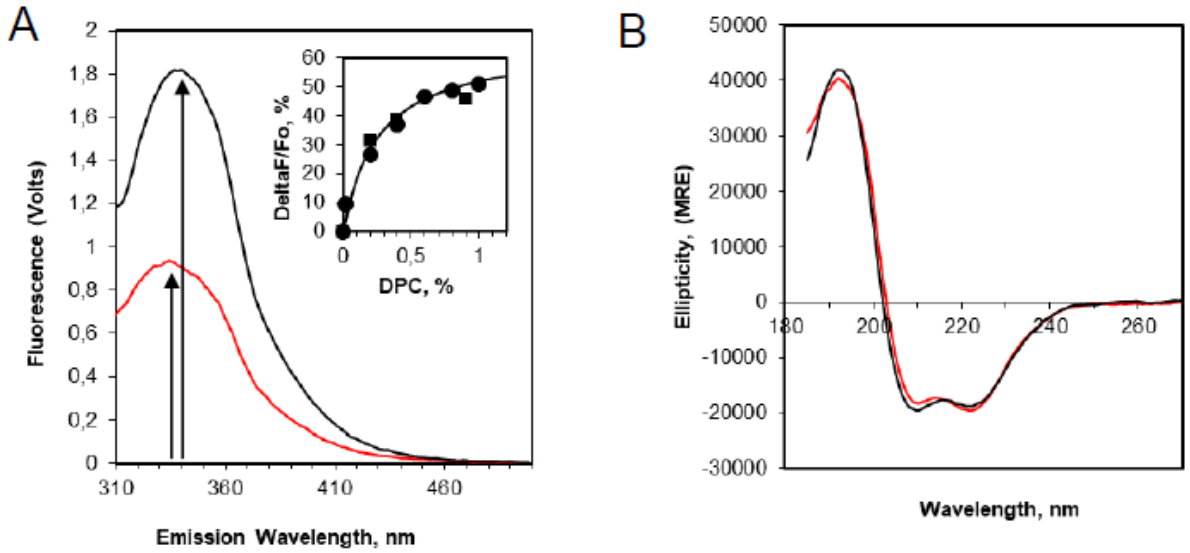

Figure 2: Intrinsic fluorescence and circular dichroism changes of *Bc*TSPO in the presence of SDS and DPC (red and black lines, respectively). (**A**) Trp emission fluorescence spectra with an excitation of 290 nm of *Bc*TSPO (5 µM) in 0.2% SDS and upon further addition of DPC up to a concentration of 1% w/v. Fluorescence maxima were observed at the wavelengths of 337 and 340 nm for SDS and DPC, respectively. Inset shows titration of the relative fluorescence as a function of added DPC concentration that gives an EC50 of 0.2%. The symbols correspond to the experimental data whereas the continuous solid line represents a linear regression curve. (**B**) Circular dichroism spectra of concentrated *Bc*TSPO purified in SDS diluted (2.4 µM) in the phosphate buffer containing either 0.2% SDS or 0.1% DPC.

Figure 3

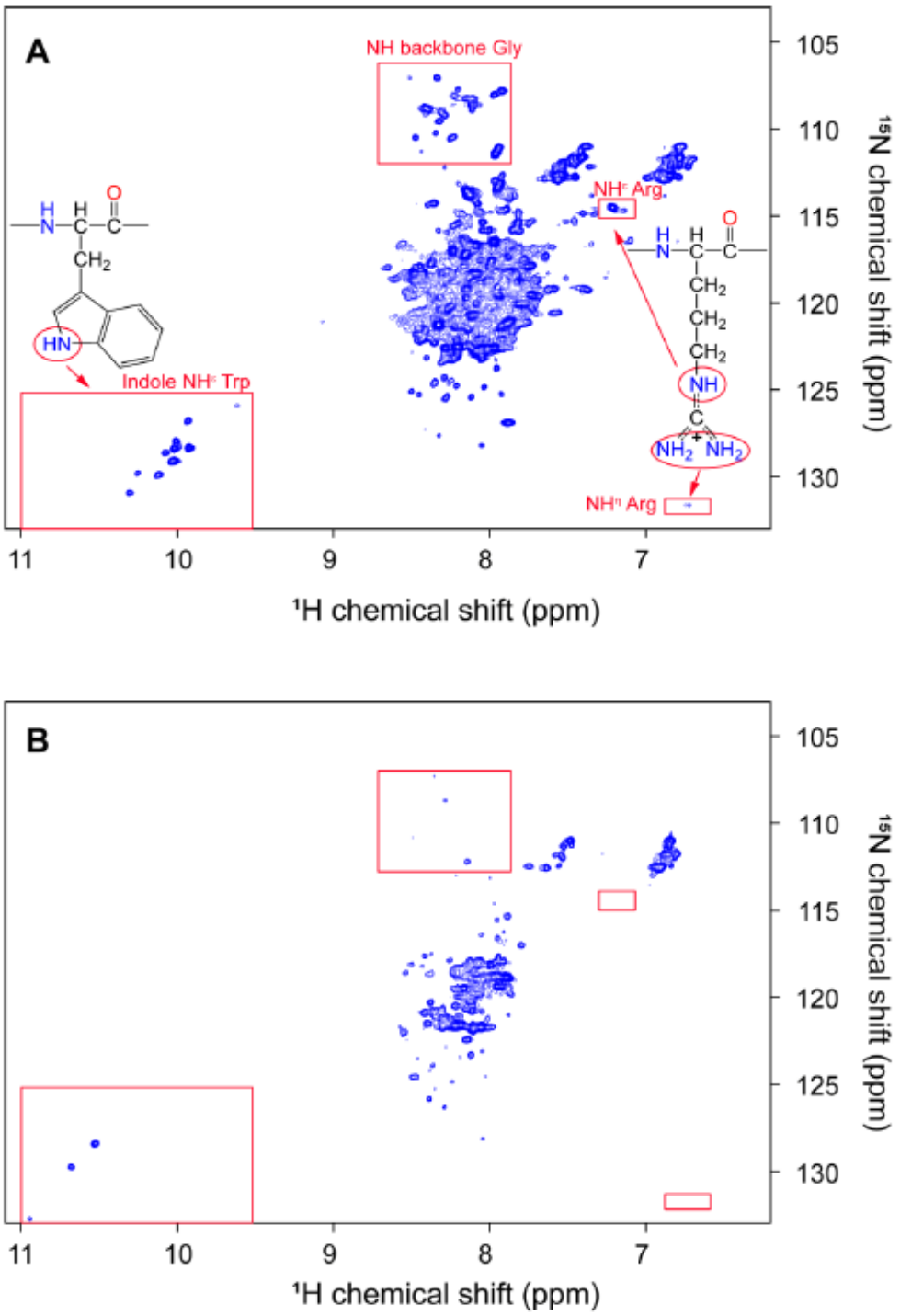

Figure 3: 2D ^{1}H - ^{15}N HSQC spectra of ^{15}N-labelled *Bc*TSPO (120 µM) purified in 0.2% SDS (**A**) and upon further addition of 5% DPC detergent (**B**). Red boxes highlight regions characteristic of specific amino acids: Glycine (backbone correlations), Arginine and Tryptophan (sidechain correlations). The spectra have been recorded at 40 °C under the same experimental conditions and have been processed in both dimensions with a squared cosine function. The base contour level was 2.6 10^{4} which represents ~16 % of the maximum intensity in 0.2% SDS and ~8% in 5% DPC, respectively with 20 levels spaced by 1.13 increment.

Figure 4

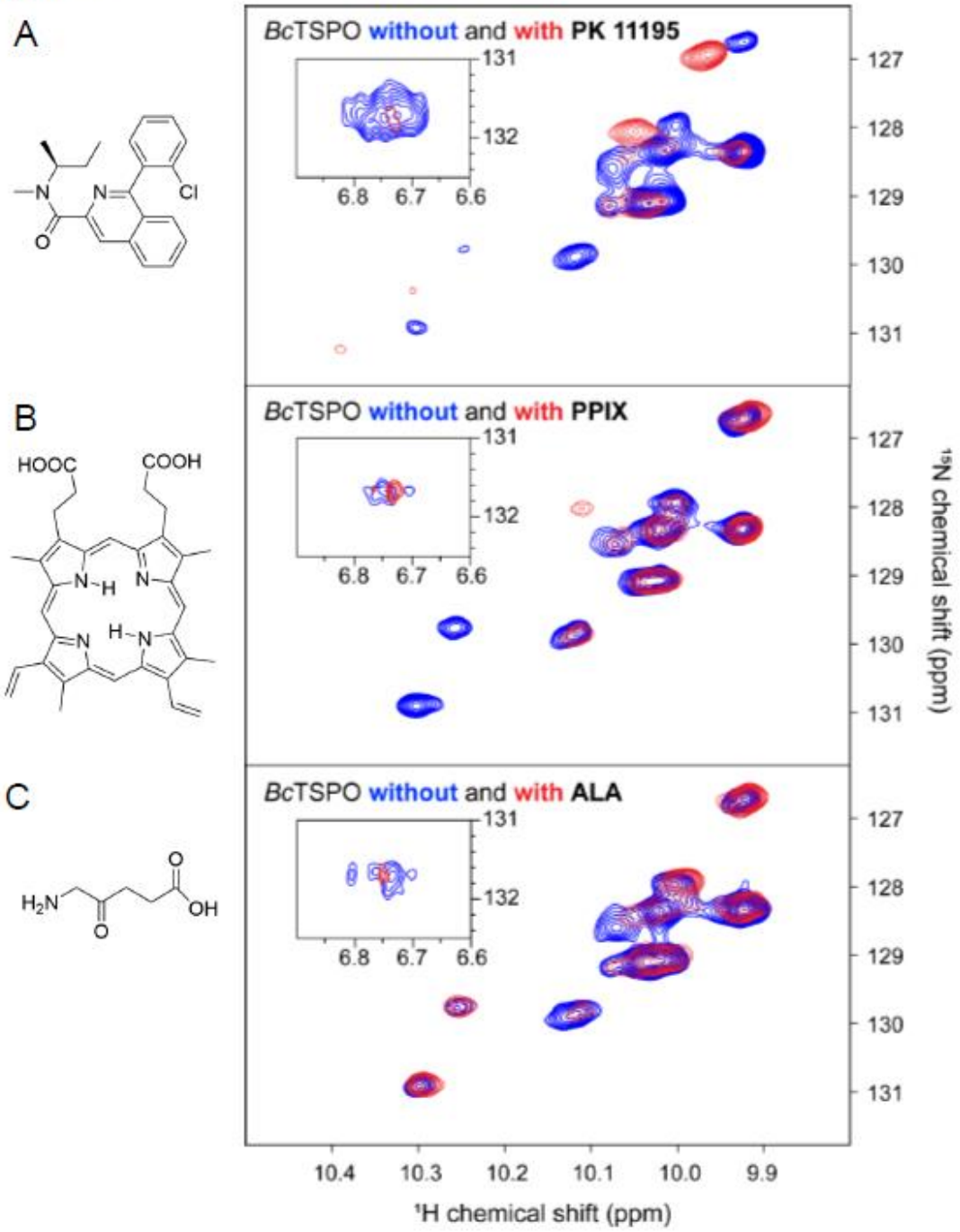

Figure 4: Indole tryptophan region of 2D ^{1}H - ^{15}N HSQC spectra of ^{15}N-labelled *Bc*TSPO purified in 0.2% SDS illustrating the effect of different ligand (blue and red, without and with ligand, respectively): (**A**) PK 11195, (**B**) PPIX, (**C**) ALA. In **A** and **B** the concentration of *Bc*TSPO was 100 µM whereas in **C** the protein concentration was 200 µM. For all conditions, protein-ligand ratio have been chosen in line with ligand solubility (5, 2.4 and 1 for PK 11195, PPIX and ALA, respectively). Insets show the effects of ligands on guanidinium resonance of the single arginine of *Bc*TSPO.

Figure 5

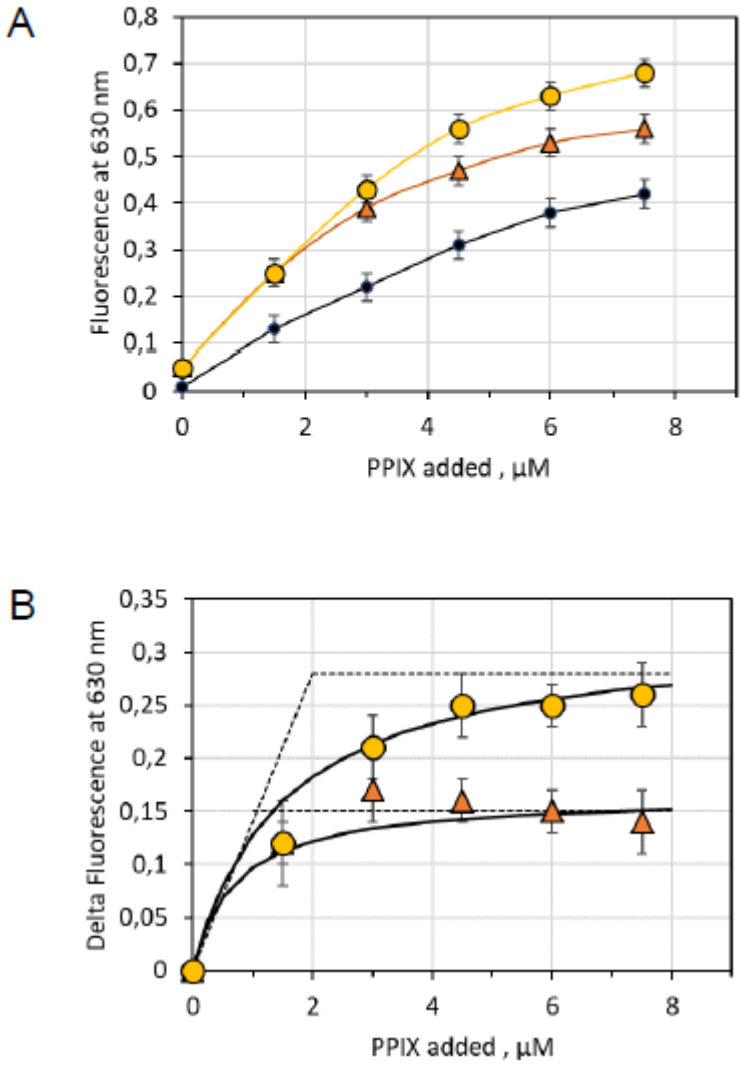

Figure 5: PPIX fluorescence titration in the presence and in the absence of *Bc*TSPO. 2 mL of 10 mM sodium phosphate buffered at pH 6.5 and containing 0.2% SDS was placed in a quartz cuvette equipped with a stirrer to maintain solution homogeneous. (**A**) Fluorescence emission intensity increases at 630 nm upon sequential addition of PPIX with an excitation at 405 nm. The concentration of *Bc*TSPO was 0, 1.0 and 2.0 µM for black circles, orange triangles and yellow circles, respectively. (**B**) Delta of fluorescence intensity in the presence of *Bc*TSPO corrected from PPIX fluorescence in the absence of the protein. Dashed lines show the concentration needed to saturate the protein, i.e. 1.0 and 2.0 µM of PPIX, suggesting a mole to mole stoichiometry. The continuous solid lines are linear regression curves (see Material and methods) corresponding to an apparent association constant, K_{app}, of 0.7 and 1.5 µM, respectively.

Figure 6

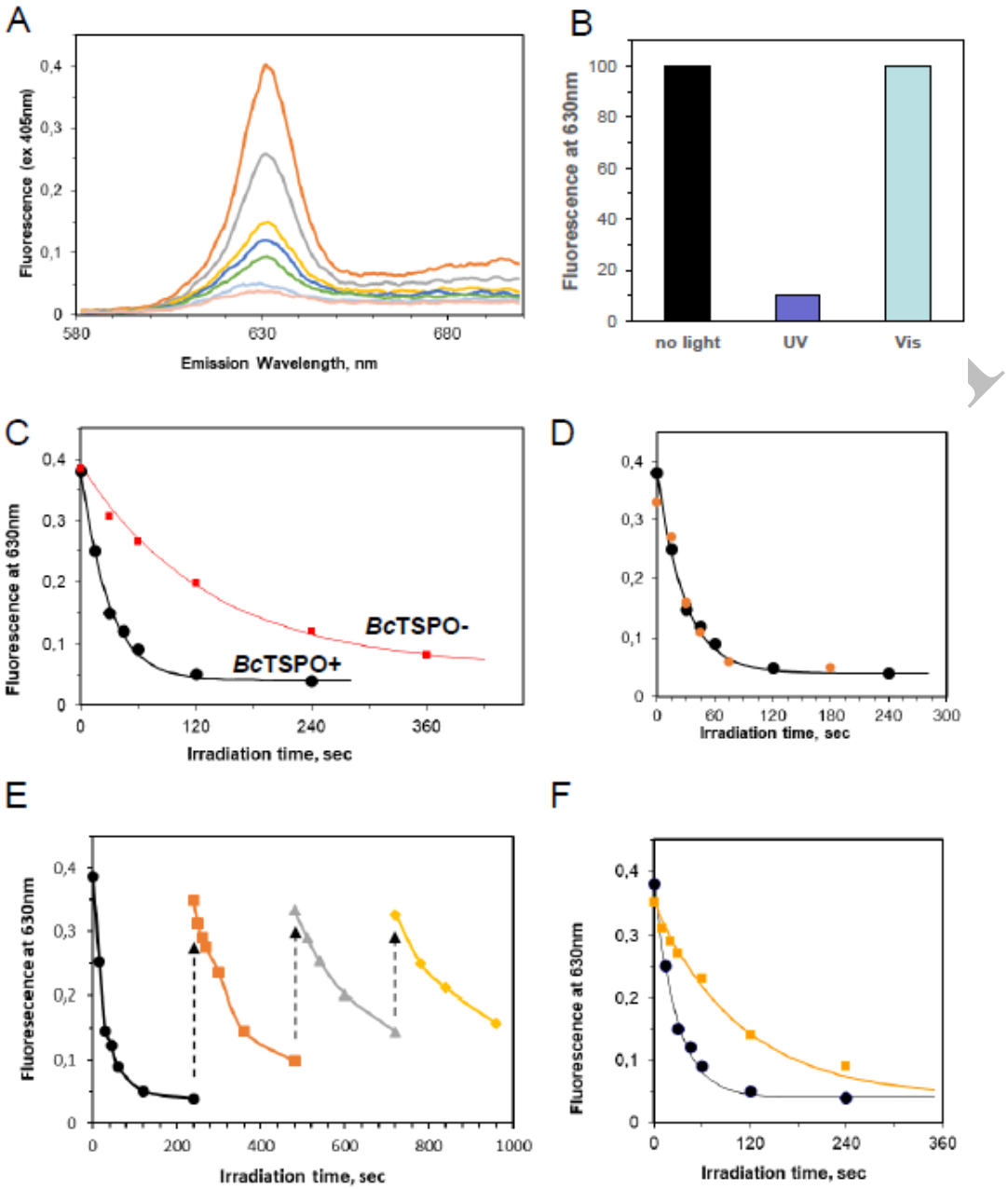

Figure 6: Light dependent PPIX fluorescence decrease. 2 mL of 10 mM sodium phosphate buffered at pH 6.5 containing 0.2 % SDS was placed in a quartz cuvette equipped with a stirrer to maintain solution homogeneous. (**A**) PPIX (3 µM) fluorescence decay (emission spectrum with an excitation at 405 nm) upon UV irradiation times of 0, 15, 30, 45, 60, 120 and 240 s (orange, grey, yellow, blue, green, cyan and pink, respectively). (**B**) Light dependence of PPIX fluorescence decrease. (**C**) PPIX (3 µM) fluorescence decay upon UV irradiation time in the absence (red squares) or in the presence of 2.5 µM of *Bc*TSPO (black circles). (D) Same as in panel C but in a phosphate medium containing either SDS or DPC 0.2% (Black or orange circle, respectively) with *Bc*TSPO. (**E**) Sequential addition of PPIX (3 µM) shows a reduction of the reaction rate. (**F**) Overlay of sequential PPIX fluorescence decay induced by UV irradiation (black circles, first addition, orange squares second addition).

Figure 7

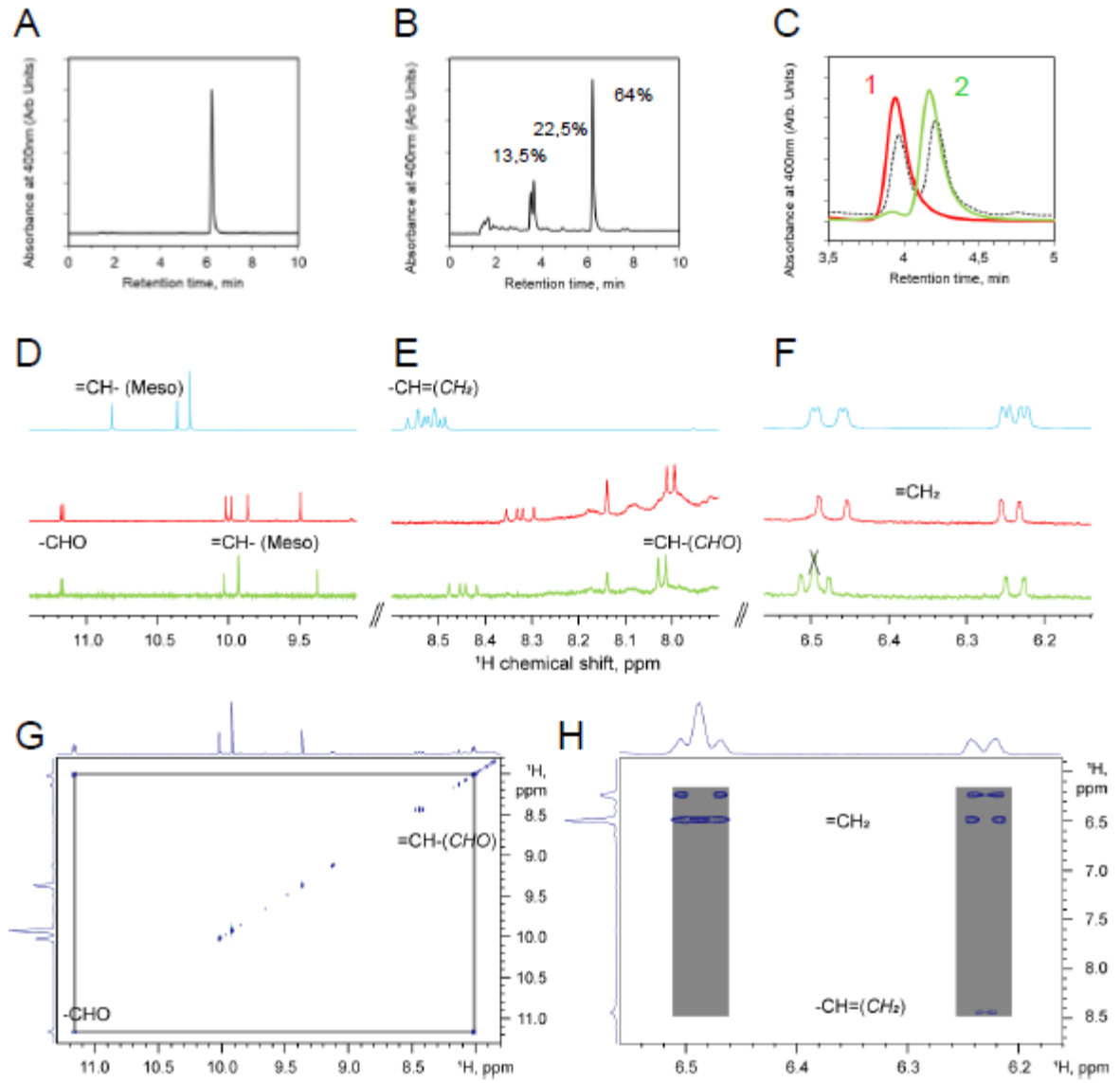

Figure 7: Characterization of irradiated PPIX compounds. HPLC of (**A**) pure PPIX, (**B**) irradiated PPIX with fractions of the total area next to the peaks. (**C**) Isolated peaks 1 and 2 in red and green, respectively. Dotted line underneath shows the two peaks before separation as in panel B. (**D**, **E** and **F**) NMR characterization of the PPIX. 1D ^{1}H spectra of pure PPIX and purified peaks 1 and 2 in cyan, red and green, respectively. Panel D shows the ^{1}H resonances corresponding to the 4 -CH= protons (Meso) of the tetrapyrrolic ring, as well as the appearance of the aldehyde function due to reaction of vinyl groups with reactive oxygen. Panel E highlights the modification of the remaining vinyl and the appearance of one =CH moiety linked to aldehyde whereas panel F shows the disappearance of one vinyl in the peaks 1 and 2. (**G** and **H**) Excerpts from the 2D ^{1}H - ^{1}H TOCSY spectrum of peak 1 enabling the characterization of the =CH–CHO moiety and the remaining vinyl group.

Figure 8

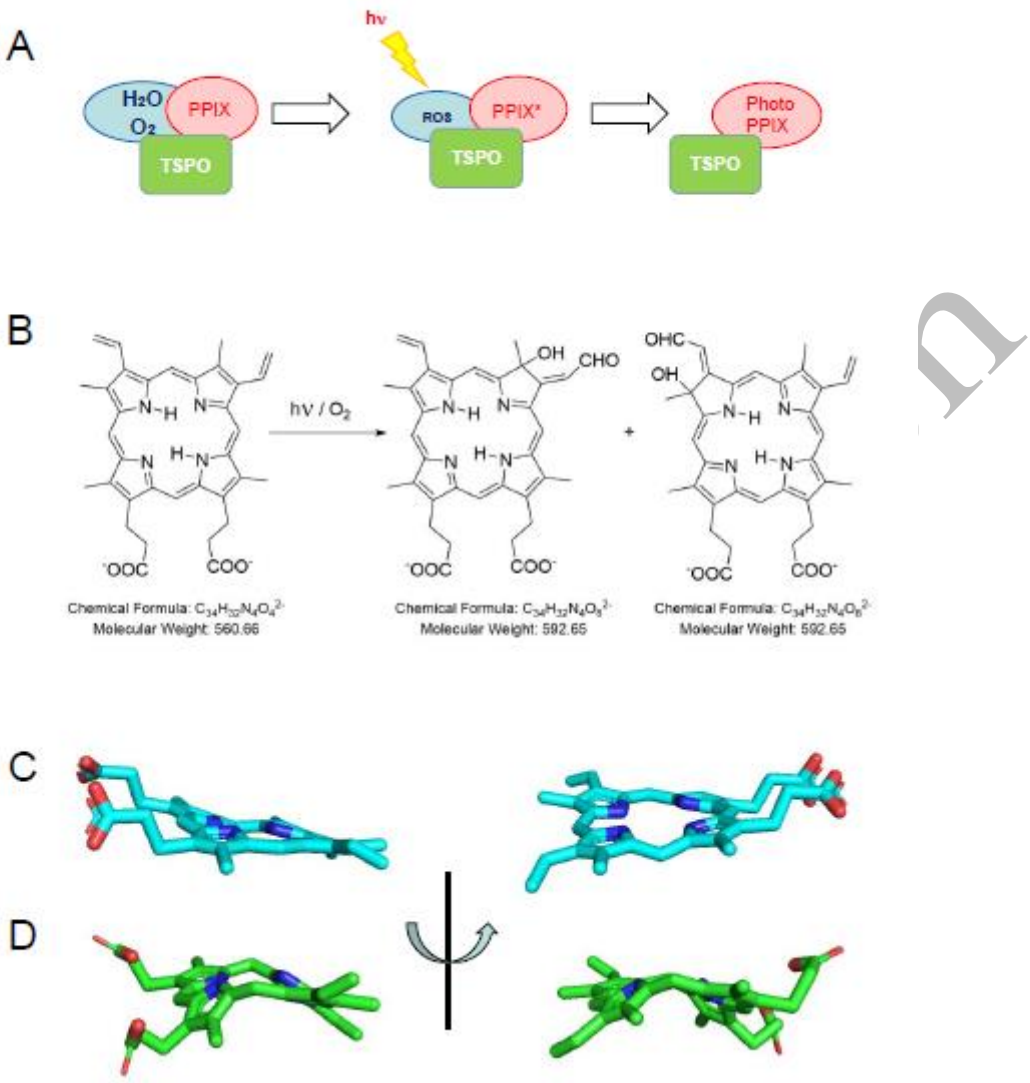

Figure 8: Interpretation of the mechanism leading to PPIX fluorescence breakdown in the presence of *Bc*TSPO. (**A**) Catalytic mechanism. (**B**) Aldehyde formation reaction through oxygen and UV irradiation. (**C**) Atomic structure of porphyrin bound to cytochrome c peroxidase (PDB code 1Z53) and (**D**) partially degraded form of PPIX in crystals of *Rs*TSPO (PDB code 5DUO).

Figure 9

A

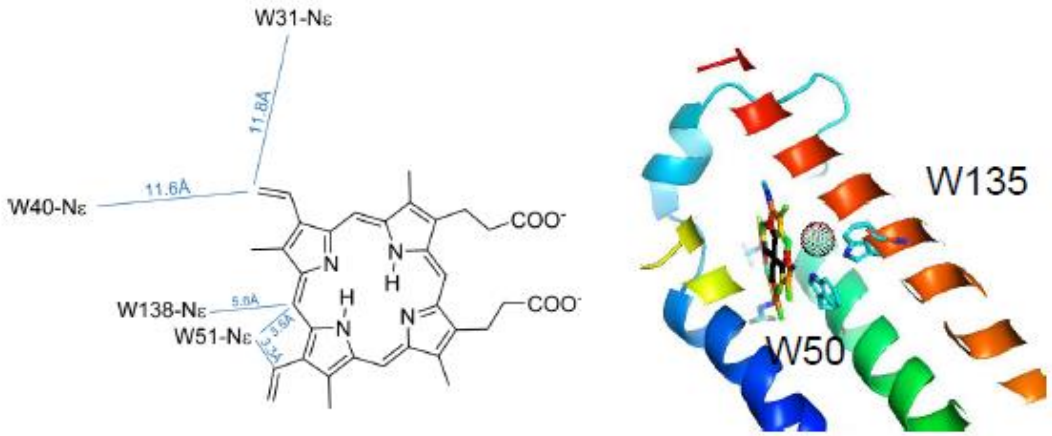

B

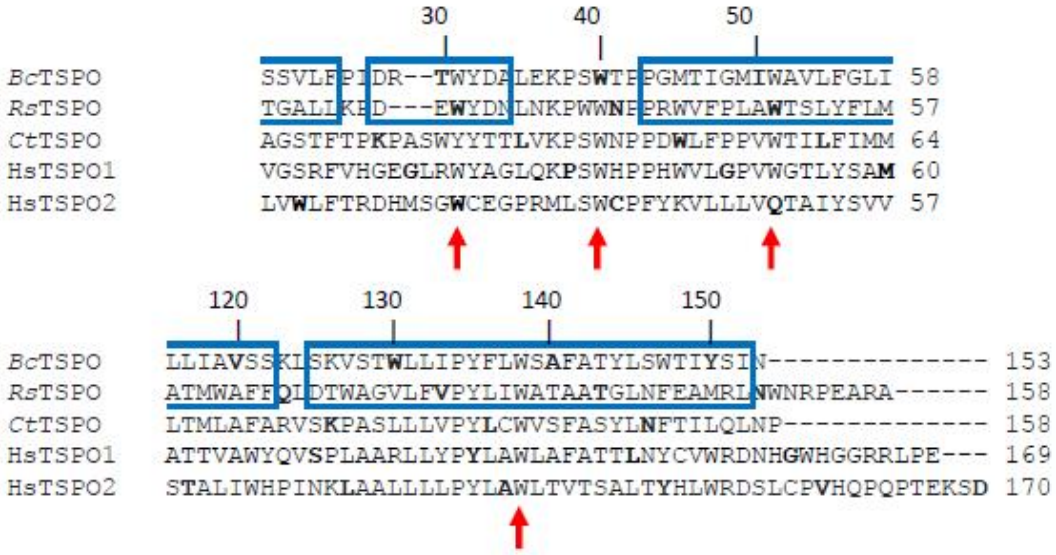

Figure 9: (**A**) Left, Potential amino acids involved in the binding and catalysis of PPIX by *Bc*TSPO (adapted from [6]). Right, inside view of heme in *Rs*TSPO (PDB code 8E7W). W50-Nε and W135-Nε of *Rs*TSPO are located to the closest CH Meso of heme at 3.5 and 5.9 Å, respectively and closest vinyl at 5.2 and 6.7 Å, respectively; among the various water molecules present in the binding cavity, the closest one is at ~6 Å of heme on the same side of W50 and W135 side chain. (**B**) Amino acid sequence alignment given in one-letter code and identified by species abbreviations: *Bc, Bacillus cereus; Rs, Rhodobacter sphaeroides; Ct, Chlorobium tepidum;* Hs, *Homo sapiens*. Bold amino acids correspond to tenth within the sequence. Blue boxes correspond to helical structures of transmembrane domains or loop.

Figure 10

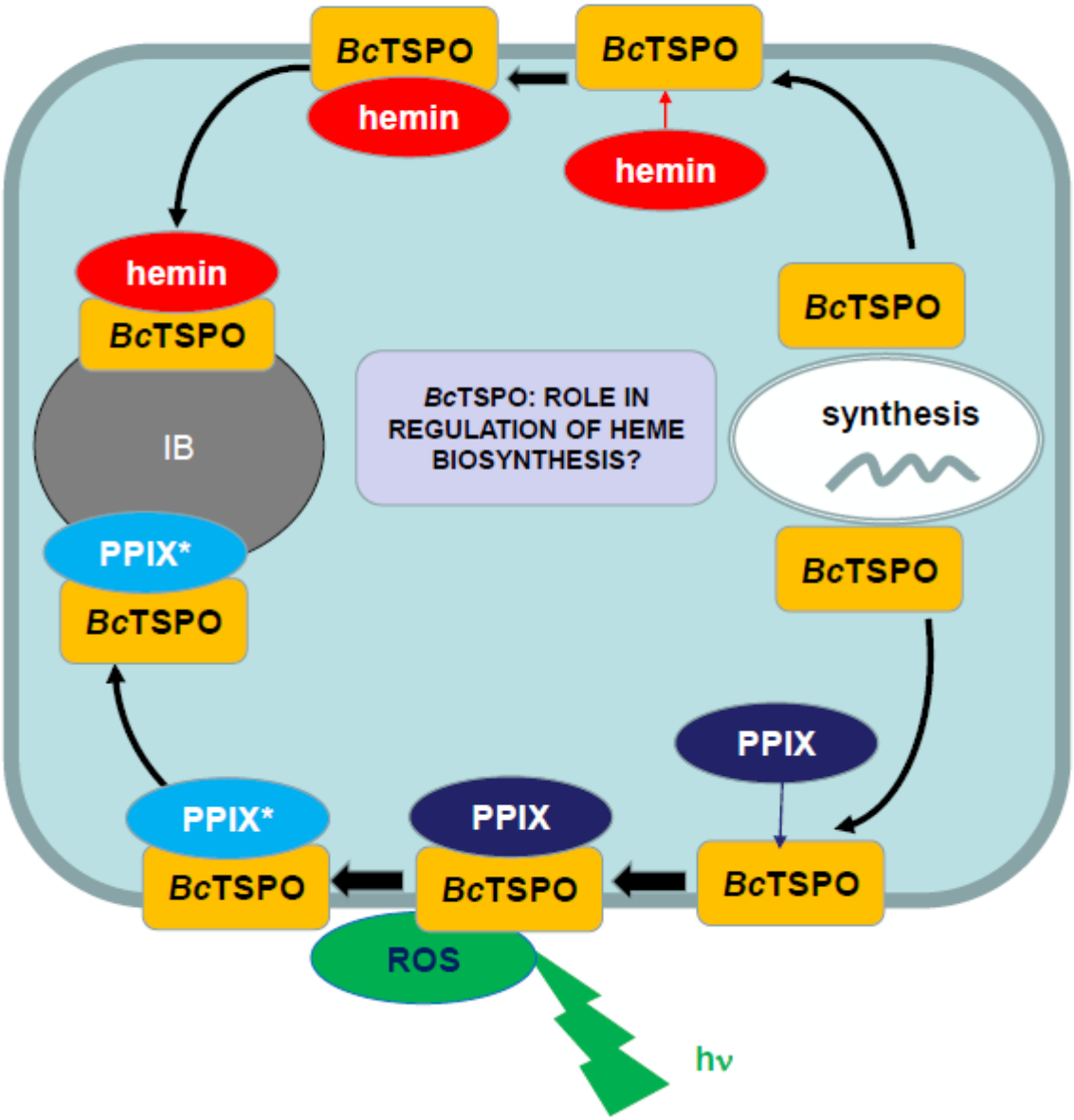

Figure 10: Recombinant *Bc*TSPO is synthesized and addressed to the plasma membrane of the *E. coli* bacteria. Hemin present in the bacteria binds to the *Bc*TSPO and the hemin-*Bc*TSPO complex is further addressed to the inclusion body. When *Bc*TSPO binds PPIX and is subjected to UV irradiation in the presence of oxygen it generates a modified PPIX (PPIX*). These two processes (hemin binding and PPIX degradation) raise the question of the potential role of TSPO in the metabolism of heme or its PPIX intermediate regulation.

Figure S1

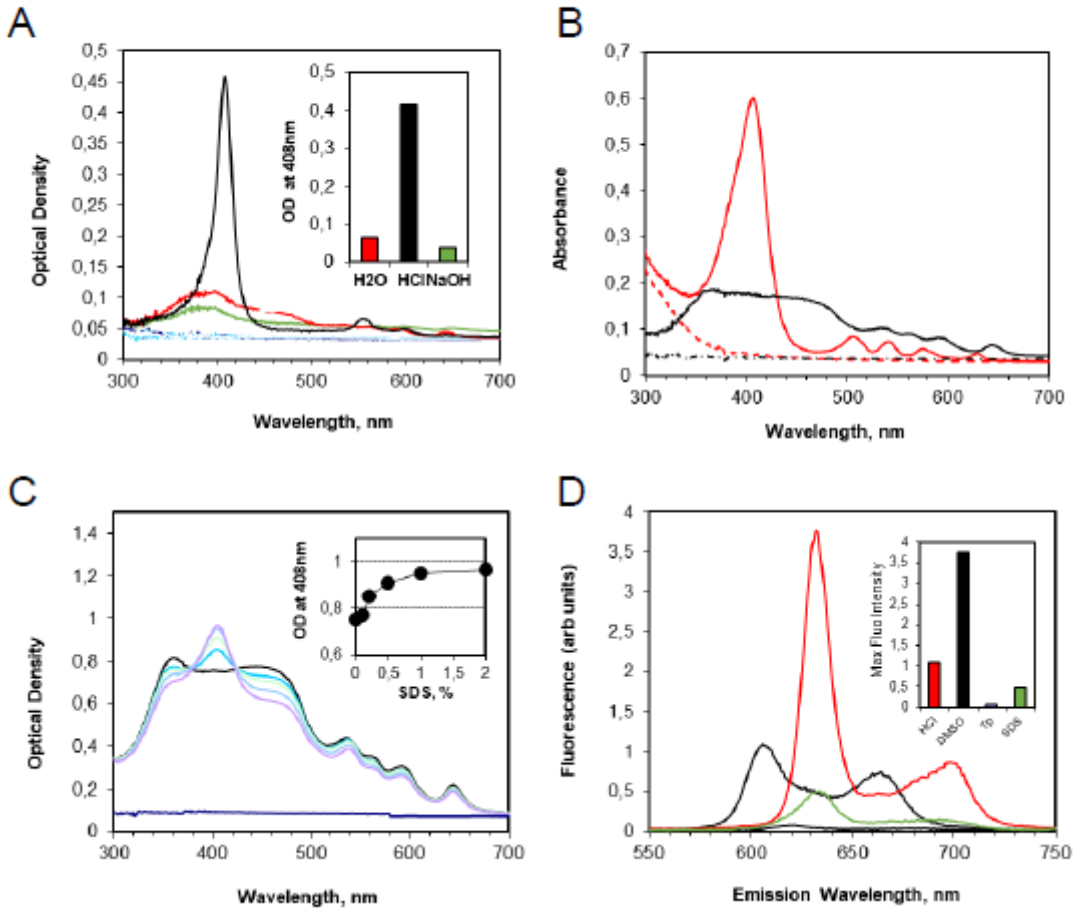

Figure S1: (**A**) Absorbance spectra of PPIX (3 µM) in various media (water, 1 M HCl and 1 M NaOH in red, black and green lines, respectively). Relative intensity at 408 nm is shown in the inset. (**B**) Absorbance spectra of PPIX (3 µM) in phosphate buffer (10 mM at pH 6.5) or pure DMSO (black and red lines, respectively). (**C**) Absorbance spectra of PPIX (3 µM) in phosphate buffer (10 mM at pH 6.5) and various SDS concentrations. The increase in the maximal intensity at 408 nm is shown in the inset. (**D**) Emission fluorescence spectra of PPIX (3 µM) in various media (1 M HCl, pure DMSO, phosphate buffer (10 mM at pH 6.5) without or with SDS in red, black, blue and green lines, respectively). The relative intensity at 608, 633, 622 and 634 nm for HCl, DMSO, phosphate buffer without or with SDS is shown in the inset.

Figure S2

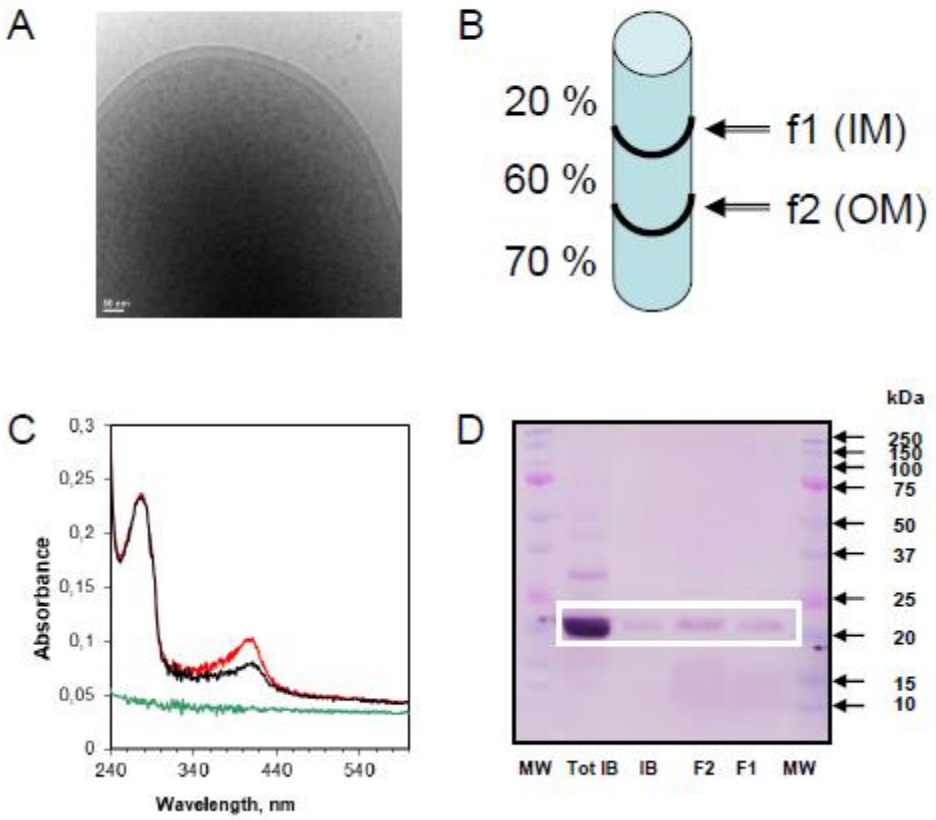

Figure S2: Localization of recombinant *Bc*TSPO in the bacterial membrane. (**A**) Cryo-electron microscopy image (scale bar 50 nm) of intact *E. coli* bacteria shows the inner membrane (IM) and outer membrane (OM). (**B**) Nonlinear sucrose gradient has been used to separate the IM (f1) from the OM (f2) that are recovered at the bottom of 20 and 60 %, respectively. (**C**) Absorbance spectra of the two collected fractions (f1 and f2 in black and red respectively) reveal the presence of hemin bound. (**D**) Western blot of the two fractions (f1 and f2) and inclusion body (purified and total). White box highlights *Bc*TSPO monomer.

Figure S3

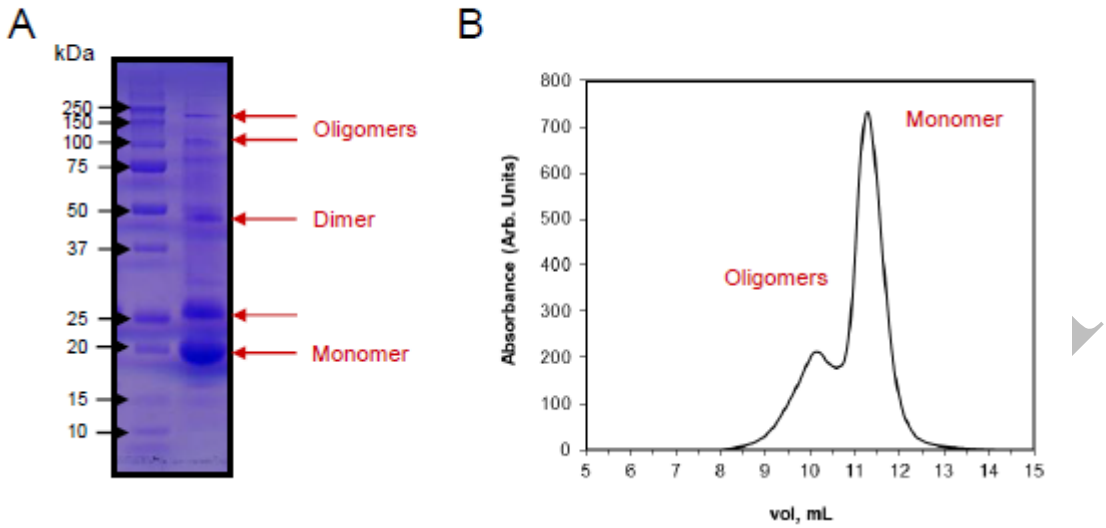

Figure S3: Oligomers of *Bc*TSPO. (**A**) SDS-PAGE of *Bc*TSPO purified from IB in a M9 culture in the presence of [^{15}N] ammonium sulfate shows, when highly loaded, not only major band corresponding to monomer, but also bands of higher molecular weight corresponding to oligomers of *Bc*TSPO. (**B**) Size exclusion chromatography reveals the presence of two peaks, the major corresponding to the monomer and the other to the oligomers.